The Astronomical Journal, 152:75 (16pp), 2016 September doi:10.3847/0004-6256/152/3/75

A WIDE-FIELD SURVEY FOR TRANSITING HOT JUPITERS AND ECLIPSING PRE-MAIN-SEQUENCE BINARIES IN YOUNG STELLAR ASSOCIATIONS*

Ryan J. Oelkers[1,6], Lucas M. Macri[1], Jennifer L. Marshall[1,2], Darren L. DePoy[1,2], Diego G. Lambas[3,4], Carlos Colazo[3], and Katelyn Stringer[1,5]

[1] George P. and Cynthia W. Mitchell Institute for Fundamental Physics and Astronomy, Department of Physics and Astronomy, Texas A&M University, College Station, TX 77843, USA; ryan.j.oelkers@vanderbilt.edu
[2] Charles R. and Judith G. Munnerlyn Astronomical Laboratory, Texas A&M University, College Station, TX 77832, USA
[3] Observatorio Astronómico, Universidad Nacional de Córdoba, Córdoba, Argentina
[4] Instituto de Astronomía Teórica y Experimental, IATE-CONICET, Córdoba, Argentina
[5] Department of Physics and Astronomy, Middle Tennessee State University, Murfreesboro, TN 37132, USA
Received 2016 May 24; revised 2016 June 3; accepted 2016 June 3; published 2016 September 6

ABSTRACT

The past two decades have seen a significant advancement in the detection, classification, and understanding of exoplanets and binaries. This is due, in large part, to the increase in use of small-aperture telescopes (<20 cm) to survey large areas of the sky to milli-mag precision with rapid cadence. The vast majority of the planetary and binary systems studied to date consists of main-sequence or evolved objects, leading to a dearth of knowledge of properties at early times (<50 Myr). Only a dozen binaries and one candidate transiting Hot Jupiter are known among pre-main-sequence objects, yet these are the systems that can provide the best constraints on stellar formation and planetary migration models. The deficiency in the number of well characterized systems is driven by the inherent and aperiodic variability found in pre-main-sequence objects, which can mask and mimic eclipse signals. Hence, a dramatic increase in the number of young systems with high-quality observations is highly desirable to guide further theoretical developments. We have recently completed a photometric survey of three nearby (<150 pc) and young (<50 Myr) moving groups with a small-aperture telescope. While our survey reached the requisite photometric precision, the temporal coverage was insufficient to detect Hot Jupiters. Nevertheless, we discovered 346 pre-main-sequence binary candidates, including 74 high-priority objects for further study.

Key words: binaries: eclipsing – planets and satellites: detection – stars: pre-main sequence

Supporting material: machine-readable tables

1. INTRODUCTION

The first planet to be detected using the transit method (Charbonneau et al. 2000; Henry et al. 2000) sparked an interest in using the technique on a massive survey scale. Over the past seven years, *Kepler* and *CoRoT* have dominated the field of transiting exoplanet detection, with *Kepler* alone yielding 962 confirmed planets and nearly another 3786 candidates (Exoplanet Orbit Database; Baglin et al. 2006; Borucki et al. 2010). The rush to detect and categorize numerous planet candidates has led to the discovery of many unexpected objects whose origins have yet to be fully explained. Of particular interest are Hot Jupiters (hereafter HJs), which were among the first extra-solar planets (hereafter exoplanets) to be detected (Mayor & Queloz 1995). Their large mass (close to that of Jupiter, $\sim 300\,M_{\oplus}$) and short orbital periods ($P < 10$ days) present a challenge to the extant theories of planet formation, many of which were based on the properties of our own solar system. The leading hypothesis to explain the existence of HJs is that they formed beyond the snow line of their proto-planetary disks ($\geqslant$4 AU for a Sun-like star) before migrating inwards (Ida & Lin 2008). However, the timescale for this process has yet to be determined observationally or fully explained theoretically.

Few wide-field, exoplanet surveys have focused on distinct stellar groups or regions for specific science objectives. The second/current phase of the *Kepler* mission (called *K2*) has a wide variety of science goals including the study of young stars and exoplanets, active galactic nucleus variability, asteroseismology, and supernovae (Howell et al. 2014). In contrast, most ongoing ground-based surveys (such as HAT, KELT, and WASP; Bakos et al. 2002; Pollacco et al. 2006; Pepper et al. 2007) target individual bright stars over the entire sky. A dedicated search of young stellar associations is necessary to fully chronicle the formation and migration of HJs.

An excellent understanding of circumstellar disk formation, accretion, and dissipation is critical to establish the timescales for planet formation and migration. Yet, the failure to discover authentic HJs around pre-main-sequence stars (hereafter PMS) is in sharp contrast with the expectations from migration models (Yu et al. 2015). The expectation from these models is that planet migration would occur in <10 Myr given the time it takes for a typical planetary disk to form, accrete, and dissipate (Mamajek 2009). While some theorists have suggested an in situ formation for these objects, they have yet to fully explain how they could retain their primary atmosphere in the warmer environment in front of the snow line (Ida & Lin 2008; Batygin et al. 2015). Planet scattering is also supported by the wide range of misaligned stellar-spin–orbit angles observed among known HJs (Anderson et al. 2016). In this scenario, a large Jupiter-sized planet forms with a similar mass outer companion. These two objects experience a Kozai scattering

* This paper includes data taken at The McDonald Observatory of The University of Texas at Austin.
[6] Current address: Department of Physics and Astronomy, Vanderbilt University, Nashville, TN 37235, USA.

Table 1
Observation Log

Young Stellar Association	Center of the Master Frame		Number of Useful Hours	Number of Baseline Days	Stars in the Master Frame
	R.A. (hr)	Decl. (deg)			
USco	16:05:42.4	−24:25:59	97.8	435	104845
IC 2391	08:38:37.6	−53:16:31	36.7	169	108964
η Cha	08:43:48.0	−79:02:07	75.6	320	81046

and the smaller body is ejected while the larger body migrates toward the host star. Currently, only one T-Tauri star (∼3 Myr) is known which possibly hosts an HJ (van Eyken et al. 2012), but this claim is hotly debated (Ciardi et al. 2015; Kamiaka et al. 2015; Yu et al. 2015). Therefore, the most reasonable test of planetary migration timescales would be a significant increase in the number of detected young HJ candidates.

Searches for young, transiting HJs would also be particularly sensitive to the detection of pre-main-sequence eclipsing binaries (hereafter PMBs). Precise and accurate measurements of stellar masses and radii at diverse ages, obtained via double-lined eclipsing binaries, provide the most rigorous tests of stellar evolution models (Torres et al. 2010; Baraffe et al. 2015). Presently, the vast majority of the systems that have been properly characterized contain main-sequence or evolved objects. In contrast, only a dozen PMBs have been discovered and studied in depth (Morales-Calderón et al. 2012).

Studies of these few PMBs have shown significant differences with predictions, calling into question some of the assumptions adopted by the models. For example, the transformation of observed properties such as temperature and luminosity into mass and age has been shown to be discrepant by 50%–100% for stars below 1 $M_{\odot}$, an inconsistency which can only be relaxed by the use of empirical relations (Stassun et al. 2014). At a broader scale, the determination of star formation rates is very sensitive to the assumed initial mass function—a parameter that is heavily dependent on the adopted evolutionary tracks of pre-main-sequence stars and currently fails to explain the observed distribution of stellar masses (Kennicutt & Evans 2012). Hence, a significant increase in the number of well characterized young systems spanning the widest possible range of masses and ages is the best approach to test and eventually improve evolutionary models.

In this publication, we present initial results from a search for exoplanets and PMS binaries in three nearby young stellar associations using a wide-field, small-aperture telescope. Section 2 describes the instrument, targets, and observations; Section 3 details the data reduction steps; Section 4 explains the techniques used to search for variability, periodicity and eclipses; Section 5 presents our results, and Section 6 contains our conclusions.

2. SURVEY DETAILS

2.1. Instrument

Our survey instrument, nicknamed *AggieCam*, consists of an Apogee Alta F16M camera with a 4096 × 4096 pixel Kodak KAD-16083 CCD that is thermoelectrically cooled down to δT = −45°C relative to ambient. Testing of the CCD showed a dark current of 0.2 e^{-} pix^{-1} s^{-1} at temperatures of −25°C relative to ambient. The optics include a Mamiya photographic 300 mm lens with a Hoya UV and IR cut filter to restrict the wavelength range to 0.4–0.7 μm. The effective aperture size of the telescope is 53.6 mm and the total throughput of the system is near 45%. The pixel scale of the detector is $6\farcs2$ pix^{-1}, leading to a total field of view (hereafter FOV) of ∼50 sq. deg. The telescope was installed at the Estación Astrofisíca de Bosque Alegre (hereafter EABA) as part of an ongoing collaboration with the Universidad Nacional de Córdoba, which owns and operates the site.

EABA is a research and outreach observatory located at 31°.412 S, 64°.489 W at an altitude of 1350 m, ∼50 km from the city of Córdoba, province of Córdoba, Argentina. Nearly all observations were carried out remotely from the Mitchell Institute of Fundamental Physics and Astronomy at Texas A&M University in College Station, Texas. Logistical support for the instrument was provided by staff members of the Instituto de Astronomía Teórica y Experimental, Observatorio de Córdoba, and EABA.

2.2. Targets and Observations

We targeted three young stellar associations to maximize the science return from our study: IC 2391 ($\alpha = 8^{h}40^{m}$, $\delta = -53°$), the η Chamaeleontis cluster (η Cha, $\alpha = 8^{h}45^{m}$, $\delta = -79°$), and the Upper Scorpius association (USco, $\alpha = 16^{h}$, $\delta = -24°.5$). Given the spread in R.A. between IC 2391 and USco and the circumpolar nature of η Cha, we were able to make an efficient use of the camera all year long.

The USco association is a subsection of the larger Scorpius-Centarus association and it is the nearest OB association to the Sun (Preibisch et al. 2002). At a distance of 145 pc and a mean age of 11 ± 1 ± 2 Myr (Pecaut et al. 2012), it is an excellent candidate for our survey. This association was chosen specifically for its large O/B/A membership (∼100 confirmed members) which implies thousands of unconfirmed low-mass members (Rizzuto et al. 2015).

IC 2391 is a large, loose, young open cluster in Vela. Measurements of the main-sequence turnoff and the lithium depletion boundary suggest an age of 30–50 Myr, while *Hipparcos* and Tycho-2 data led Reipurth (2008) to determine the distance to this cluster to be 147 ± 5 pc. This association was chosen because of its older population; we may expect to see transiting HJs if migration timescales are constrained by disk dissipation.

Lastly, η Cha is a cluster located at a distance of 97 pc with confirmed stellar ages between 2 and 18 Myr (Mamajek et al. 1999). η Cha provides a variety of stellar ages to probe planetary formation, has a high number of confirmed T-Tauri stars, and was chosen to ensure we could observe at least one target all year.

Individual exposures were set to 60 s and were taken when a field was above an airmass of 3. Table 1 denotes the number of exposures taken and baseline of days between the first and last exposure for each field. For the remainder of this paper, we will use the abbreviated names of each target (USco, η Cha, and

IC 2391) to refer to all stars in the respective fields of view and not just the *bona-fide* members.

3. DATA ANALYSIS

3.1. Pre-processing

Each frame was pre-processed for bias subtraction, flat fielding, and residual background correction. The master bias frame was generated by median-combining 160 bias frames taken throughout the observing season. The master flat field was created by median-combining 410 sky flats taken throughout the observing season with values $\geqslant$10,000 ADU. We bias-subtracted, scaled, and median-combined the selected frames to make a temporary flat field, applied it to the images, masked any stars, and repeated the process to generate the final flat. This master flat frame was normalized by the center 2048×2048 pixels to avoid contamination by the vignetted corners of the detector.

We applied a residual background correction following the approach of Wang et al. (2013) and Oelkers et al. (2015) to remove any variations due to clouds, moonlight, or scattered light. The residual background model is constructed by sampling the sky background every 64×64 pixels over the entire detector. Bad or saturated pixels are excluded from each sky sample. A model sky is then fit inside each box and interpolated between all boxes to make a thin plate spline (Duchon 1976). We used the IDL implementation GRID_TPS to make the spline which is subtracted from the frame.

We corrected for slight drifts in tracking by carrying out aperture photometry on all images using DAOPHOT (Stetson 1987), matching the resulting star lists with DAOMATCH, and solving for the geometric transformations with DAOMASTER. We aligned the images using the bi-cubic interpolation implemented in the IDL routine POLY_WARP.

3.2. Difference Image Analysis

We used Difference Imaging Analysis (hereafter DIA; Alard & Lupton 1998) to match the point-spread function (PSF) of each science frame and a reference master image and measure changes in stellar flux. Since the PSF in our images was spatially varying, we applied a 5×5 pix, second order, Dirac-δ-function kernel across the frames (Alard 2000; Miller et al. 2008). A detailed description of the algorithm is given in Oelkers et al. (2015), and the code is publicly available from https://github.com/ryanoelkers/DIA. Stamps were taken around bright, isolated stars to solve for the kernel coefficients using the least-squares method.

3.3. Flux Extraction

We extracted the stellar flux on each differenced frame using the IDL implementation of the DAOPHOT routine APER. The aperture radius was set to 3 pix (18.″6) with a sky annulus from 5 to 7 pix (31–43.″4). These fluxes were added to the flux from the master frame, zero-pointed, and corrected for exposure time. We only selected stars located between 500 and 3500 in both (x, y) in the master frame to remove objects with poorer photometry due to vignetting. The final star lists are given in Table 2.

We used ensemble photometry to identify and remove systematic trends due to instrumental or processing effects that were present in multiple light curves. We used the Trend Fitting Algorithm (Kovács et al. 2005) as implemented in the VARTOOLS package (Hartman et al. 2008) to compensate for these systematics. We used 100–250 stars spanning a wide range of fluxes and (x, y) positions that did not exhibit any discernible variations of an astrophysical nature (e.g., eclipsing binaries, periodic variables, etc.) as templates for the trend removal.

3.4. Photometric Calibration

We determined the transformation of *AggieCam* magnitudes, obtained through a fairly wide filter, to the standard V band via observations of SA 110 (Landolt 1992) at airmass values of $1.18 < X < 2.0$. The field was selected because of the relative large number of bright standard stars in our FOV (14) which spanned a large range in color ($0.3 < B - V < 2.6$). Fluxes were extracted following the same procedure used for our science observations. We solved for the following transformation equation:

$$m_{V_{AC}} = m_{inst} + 2.5 \log_{10}(t_{exp}) + \chi + k(X - 1) + \xi(B - V) + \xi'(B - V)^2, \quad (1)$$

where $m_{V_{AC}}$ is the *AggieCam* V-band calibrated magnitude; m_{inst} is the instrumental magnitude; t_{exp} is the exposure time of the observation; χ is the zero-point offset; k is the airmass coefficient; X is the airmass of the observation; ξ and ξ' are the first- and second-order color terms, respectively; and $(B - V)$ is the color of the star in the standard B and V bands. We solved the transformation equation using the IDL routines POLY_FIT and LINFIT, finding $\chi = -7.21 \pm 0.02$, $k = -0.16 \pm 0.01$, $\xi = 0.12 \pm 0.01$ and $\xi' = 0.08 \pm 0.01$ as shown in Figure 1.

We determined the sky background at the observatory by calculating the median pixel value of each image. We find the background is fairly low for an observatory in relatively close proximity to a major metropolitan area. The lowest values were found toward the south, where the instrument was primarily pointed, when the lunar phase was <0.5. The median sky background was $V = 20.5$ mag/□″, comparable to the median value at Mauna Kea (20.7 in the same units). Figure 1 shows the normalized number of observations and their median sky background values.

3.5. Noise

One of the leading reasons PMS stars have been so poorly studied is due to their intrinsic stellar variability, which appears to be both erratic and aperiodic. This variability is likely the result of ongoing stellar contraction toward its main-sequence radius, increased spot cycle due to magnetic activity, proto-stellar disk accretion, or a combination of all these factors (Stassun et al. 2014). This variability can mask and mimic signals which are important to the understanding of the fundamental properties of stars such as determining stellar rotation rates, identifying planetary and stellar eclipses or making precise radial velocity measurements.

Studies attempting to reduce the impact of astrophysical variation in PMS stars rely on the blind whitening of light curves against suspected periodic variability (Kraus et al. 2015) or on the use of self-described, overly flexible data-driven models which de-weight variation similar to the desired signal (Wang et al. 2015). While these techniques adequately remove variation, the possibility that *bona-fide* signals will be removed is greatly

Table 2
AggieCam Stellar Library

Star ID	Coordinates J2000		V_{AC}	Metrics			Period (days)		Cluster Type
	R.A. (hr)	Decl. (deg)		*V*	*P*	*E*	LS	BLS	
U098597	16:03:30.09	−24:31:47	11.043	1	1	0	2.530870	···	STU
U038698	16:12:38.88	−23:26:56	14.804	1	1	0	1.618511	···	IRV
V027962	08:39:10.08	−55:47:08	13.040	1	1	0	129.932922	···	LTN
V046511	08:40:56.08	−55:09:34	13.663	1	1	0	0.594557	···	IRV
U048565	16:11:19.20	−26:29:15	15.174	1	1	0	1.354051	···	IRV
U089470	16:04:58.48	−26:14:12	15.433	1	1	0	3.987664	···	STU
V038184	08:35:21.32	−55:27:32	13.831	1	1	0	1.011477	···	STU
U050223	16:10:44.16	−23:03:57	14.983	1	1	0	255.915588	···	LTU
U096707	16:03:52.96	−26:48:23	13.949	1	1	0	271.910309	···	LTU
V060026	08:51:16.05	−54:38:32	12.686	1	1	0	21.655487	···	IRV
U089370	16:05:01.97	−26:58:09	14.720	1	1	0	1.022940	···	STU
C068057	09:25:32.43	−78:34:45	13.512	1	1	0	114.386337	···	LTN
U046582	16:11:26.73	−24:28:02	10.436	1	1	0	24.036270	···	STU
U057495	16:09:42.50	−24:31:03	13.074	1	1	0	6.360475	···	STU
V028652	08:34:04.63	−55:46:34	12.986	1	1	0	45.440865	···	LTN
U024137	16:15:19.63	−24:18:42	12.614	1	1	0	255.915588	···	LTU
V038671	08:29:06.09	−55:26:53	12.741	1	1	0	39.282047	···	STU
C015455	08:35:06.59	−81:31:09	11.980	1	1	0	103.316689	···	LTN
V079454	08:38:14.68	−54:07:23	13.961	1	1	0	0.174279	···	STU
U088883	16:05:06.32	−26:55:37	16.064	1	1	0	12.220644	···	STU
V081626	08:43:48.46	−54:01:37	13.038	1	1	0	0.156274	···	STU

Note. A 1 in the metric column denotes if the star passed the variability (*V*), periodicity (*P*), or eclipse (*E*) testing in Section 4. The types in the Cluster Type column are based on the five clusters described in Section 5.1.1; STU is short-term uniform periodic, IRV is infrequent variable, STN is short-term non-uniform periodic, LTU is long-term uniform variable, LTN is long-term non-uniform variable, and TRN is a transit candidate.

(This table is available in its entirety in machine-readable form.)

increased. Therefore, it is necessary to isolate and understand the source of each signal and the associated noise, prior to removal, in order to preserve the scientific integrity of the data.

We modeled the statistical uncertainty as $\sigma^2 = I_N + AI_{\rm sky} + 2A\,({\rm RN}^2) + \sigma_a^2$, where I_N and $I_{\rm sky}$ are the photon counts from the object and sky, respectively, A is the area of the photometric aperture, RN is the read noise of the detector and σ_a is the expected scintillation limit defined by Young (1967) and Hartman et al. (2005) as:

$$S = S_0 d^{-\frac{2}{3}} X^{\frac{7}{4}} e^{-h/8000} (2t_{\rm ex})^{-\frac{1}{2}}, \quad (2)$$

where $S_0 \sim 0.1$ mag, d is the telescope diameter in cm, X is the airmass, h is the altitude in m and $t_{\rm ex}$ is the exposure time in s. The values for *AggieCam* at EABA are: $d = 5.36$, $h = 1350$, $1 < X < 3$, and $t_{\rm ex} = 60$. We find $0.003 < S < 0.017$ mag, with a value of 5 mmag for the median airmass of our observations ($\langle X \rangle = 1.5$).

We measured the dispersion in each light curve, weighted by the uncertainty in aperture photometry, for a single night of observations (typically 60–360 frames) and compared these values to our noise model. We found satisfactory agreement with the simple model described above, with dispersions of 1–1.4× the scintillation limit for stars with $V_{\rm AC} < 10.9$ as shown in Figure 2.

4. SEARCHING FOR VARIABILITY, PERIODICITY, AND ECLIPSES

4.1. Classical Variability and Periodicity

We employed a combination of three variability metrics following the approach of Wang et al. (2013) and Oelkers et al. (2015). First, we computed the root mean square (hereafter rms) of all stars and the upper 2σ envelope as a function of magnitude; objects lying above this limit are likely to be genuine astrophysical variables. Next, we computed the magnitude range spanned by 90% of the data points of every light curve (hereafter Δ_{90}) and its upper 2σ envelope as a function of magnitude. Since we wished that both statistics be based on "constant" stars only and not be biased by large-amplitude variables, both envelopes were calculated in an iterative fashion.

Finally, we computed the Welch–Stetson J variability statistic (hereafter J; Stetson 1996) including the necessary rescaling of DAOPHOT errors (Kaluzny et al. 1998). J is useful to detect variability during short time spans, such as those sampled by the 60 s cadence of the *AggieCam*, since it computes the significance of photometric variability between two or three adjacent data points. J is expected to produce a distribution of values with a mean value close to zero for the "constant" stars and a one-sided tail toward positive values for the "variable" stars. We considered objects lying above the $+3\sigma$ value as variable.

We also applied a variety of cuts to our variable sample to ensure we were not contaminated by stars showing high dispersion due to systematics. We removed the 10% of stars with the lowest number of data points and we required each star to be farther than 5 pixels of a star 2 magnitudes or brighter. We *only* consider a star to be variable if it passes all three of these metrics. Figure 3 shows these techniques recovering the variable candidate U071728.

We searched each light curve for periodic signals using a Lomb–Scargle periodogram (hereafter LS; Lomb 1976; Scargle 1982) as implemented in `VARTOOLS` (Press et al. 1992;

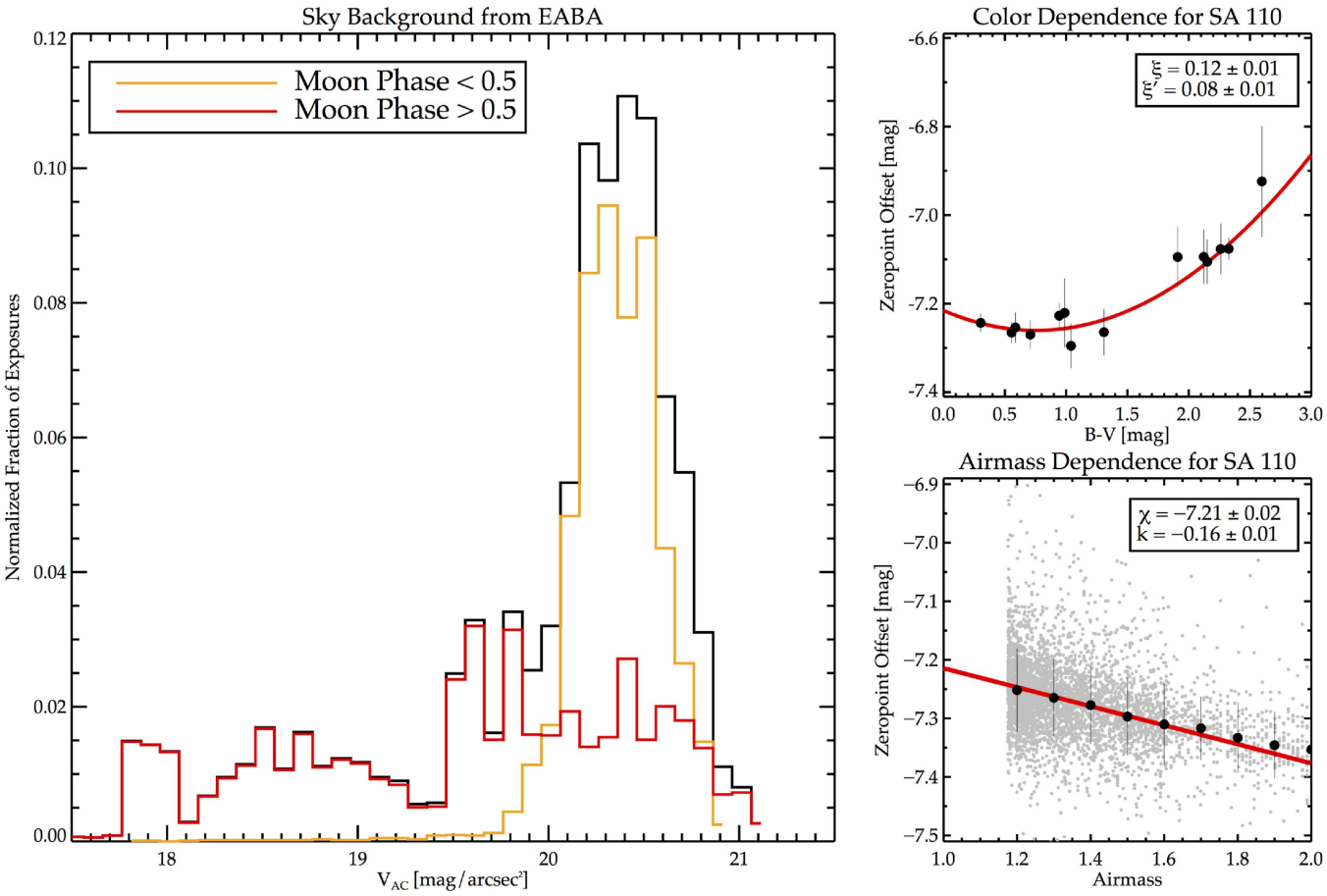

Figure 1. Left: the sky background from EABA during the survey in mag arcseconds^{-2}. The site has generally dark observing conditions especially when the moon phase is <0.5. Top right: the zero-point offset of the *AggieCam* detector as a function of $B - V$ color. Bottom right: the zero-point offset of the *AggieCam* detector as a function of airmass. All data was calibrated to Johnson–Bessell V band (Johnson & Morgan 1953; Bessell 1990) using the Landolt standard star field SA 110 (Landolt 1992) using $M_{V_{AC}} = m_{inst} + 2.5\log_{10}(t_{exp}) + \chi + k(X - 1) + \xi(B - V) + \xi'(B - V)^2$.

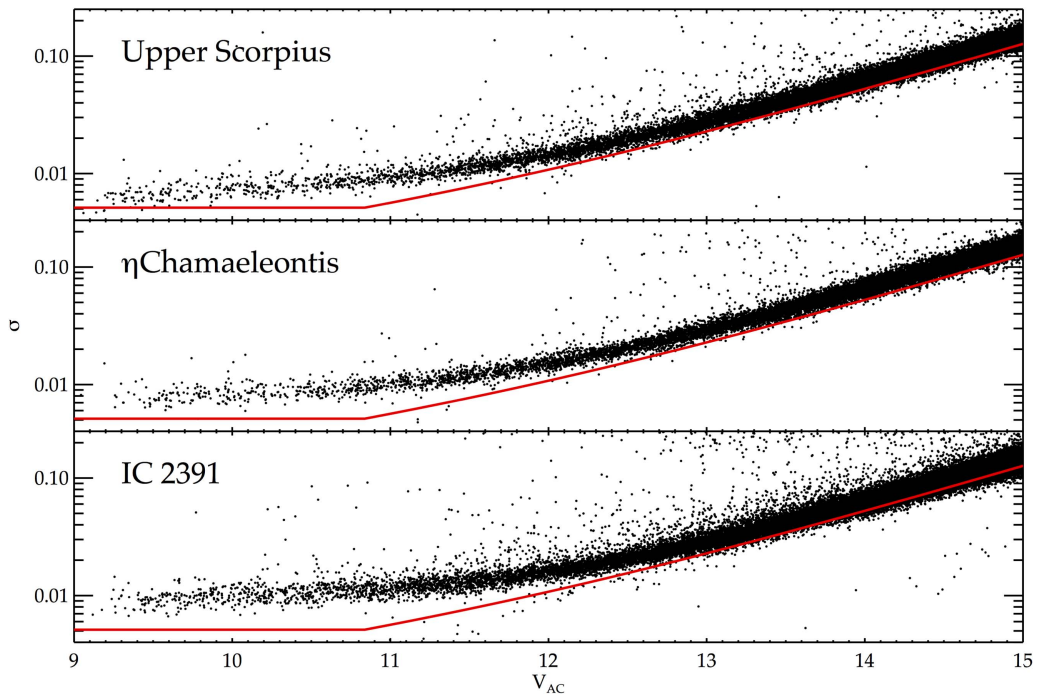

Figure 2. Achieved photometric precision of *AggieCam* from a typical day of observations. The red line denotes the expected noise from the star, sky, detector, and scintillation limit.

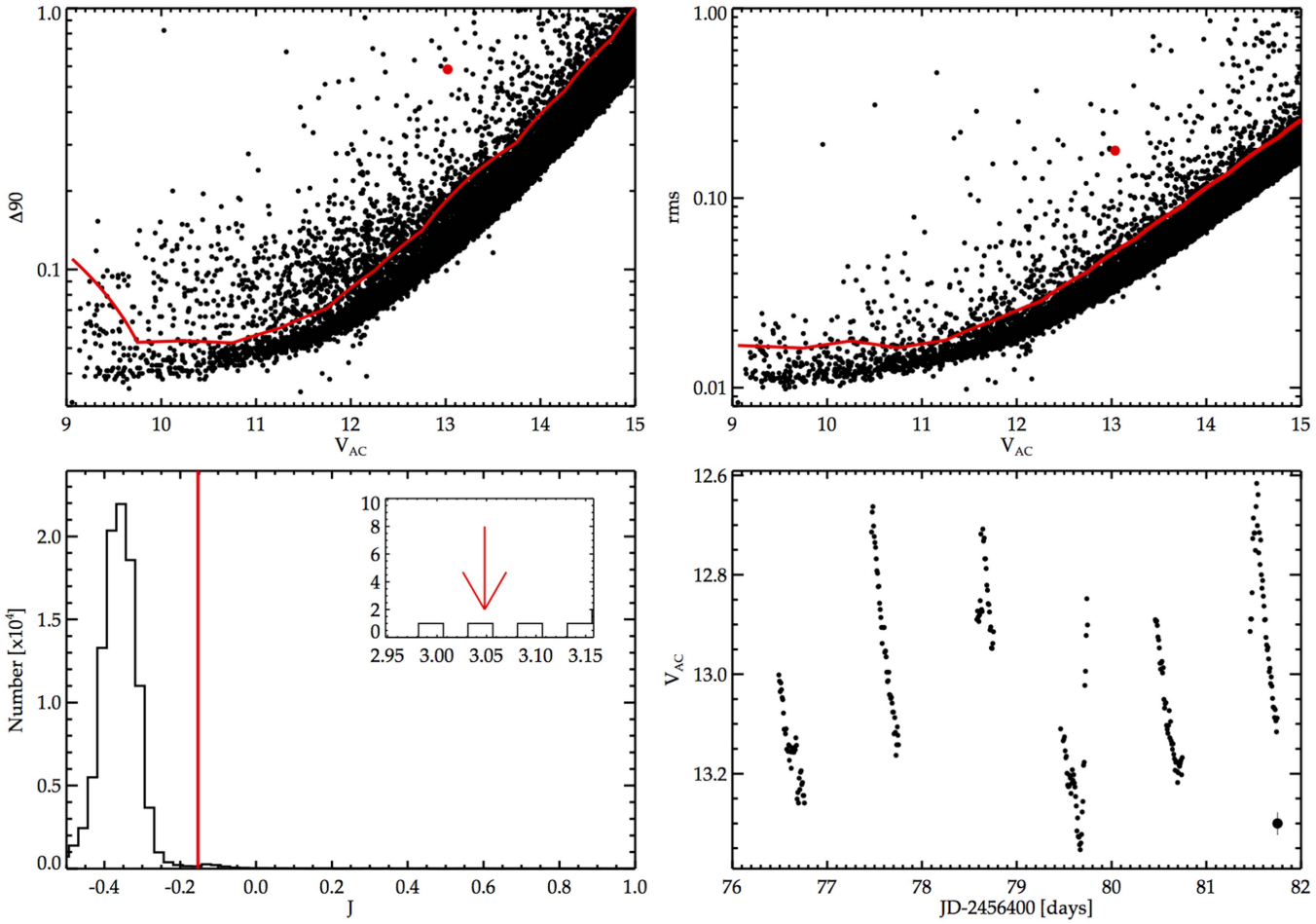

Figure 3. Variability tests used to identify variable candidates in each young stellar association. Stars lying above the red line in the top panels and to the right of the line in the bottom left panel are expected to be variable. Top left: Δ_{90} statistic with the upper 2σ quartile plotted as a red line. Top right: rms statistic with the upper 2σ quartile plotted as a red line. Bottom left: J Stetson statistic with the upper 3σ cut plotted as a red line. Bottom right: the light curve of the variable candidate U071728 from the USco field. The candidate is shown clearly passing each statistic as a red dot in the top two panels and a red arrow in the bottom left panel. The light curve is shown in 10 m bins with the size of the typical photometric error shown at the bottom right.

Hartman et al. 2008; Zechmeister & Kürster 2009). We computed the highest SNR period of each star between 0.1 day and the total number of baseline days of observation for each association. We removed periods within 0.001 day of any of the first 10 harmonics (*f, f/2, f/3, ...*) of the sidereal day (0.99726958d) to alleviate contamination from the most common observing alias. We also removed periods which were within 1 day of the lunar sidereal month, 27.32 days. We applied $+3\sigma$ cuts on the false alarm probability, $\log_{10}$(FAP), and cumulative SNR. The FAP provides an estimate on the likelihood of a true periodic signal by comparing the SNR of a specific signal to the cumulative distribution of all SNRs for each peak in the LS periodogram. Figure 4 shows these techniques recovering the periodic variable candidate U071728.

4.2. Stellar and Planetary Eclipses

We ran the box least-squares algorithm (hereafter BLS; Kovács et al. 2002) to search for eclipse-like events of the desired HJs. The signal is non-sinusoidal because the transit is only expected to occur for a very short amount of phase, typically <10% (Charbonneau et al. 2000). The BLS routine searches for signals caused by a periodic alternation between two flux levels. The probability of detecting a small, periodic, eclipse-like feature is greatly increased by iteratively searching over the parameter space of period, eclipse depth, and transit length.

We also ran a BLS search, where, prior to the search, we pre-whitened each light curve against the primary LS period between 0.1 and 10 days and its 10(9) (sub-)harmonics. We searched each light curve for transit candidates with a primary BLS period between 0.1 and 10 days with a transit length of 0.01 and 0.1 of the primary BLS period. We chose the limit of 10 days because HJs, by definition, do not have periods longer than 10 days. We allowed for 10^4 trial periods and 200 phase bins. We also adopted a number of detection thresholds that are common among exoplanet searches. We required no less than three transit events for every candidate to ensure no significant variation between the odd and even eclipses, which would suggest an eclipsing binary over a planetary transit. While typical planetary transits produce a drop in the light curve of only 1%–2%, we kept larger depth events since they could be due to other interesting objects such as brown dwarfs or eclipsing binaries.

We then subjected each light curve to criteria based on the statistics of the BLS routine. Typically, the error in ground-based milli-magnitude photometry is correlated. Because this is the

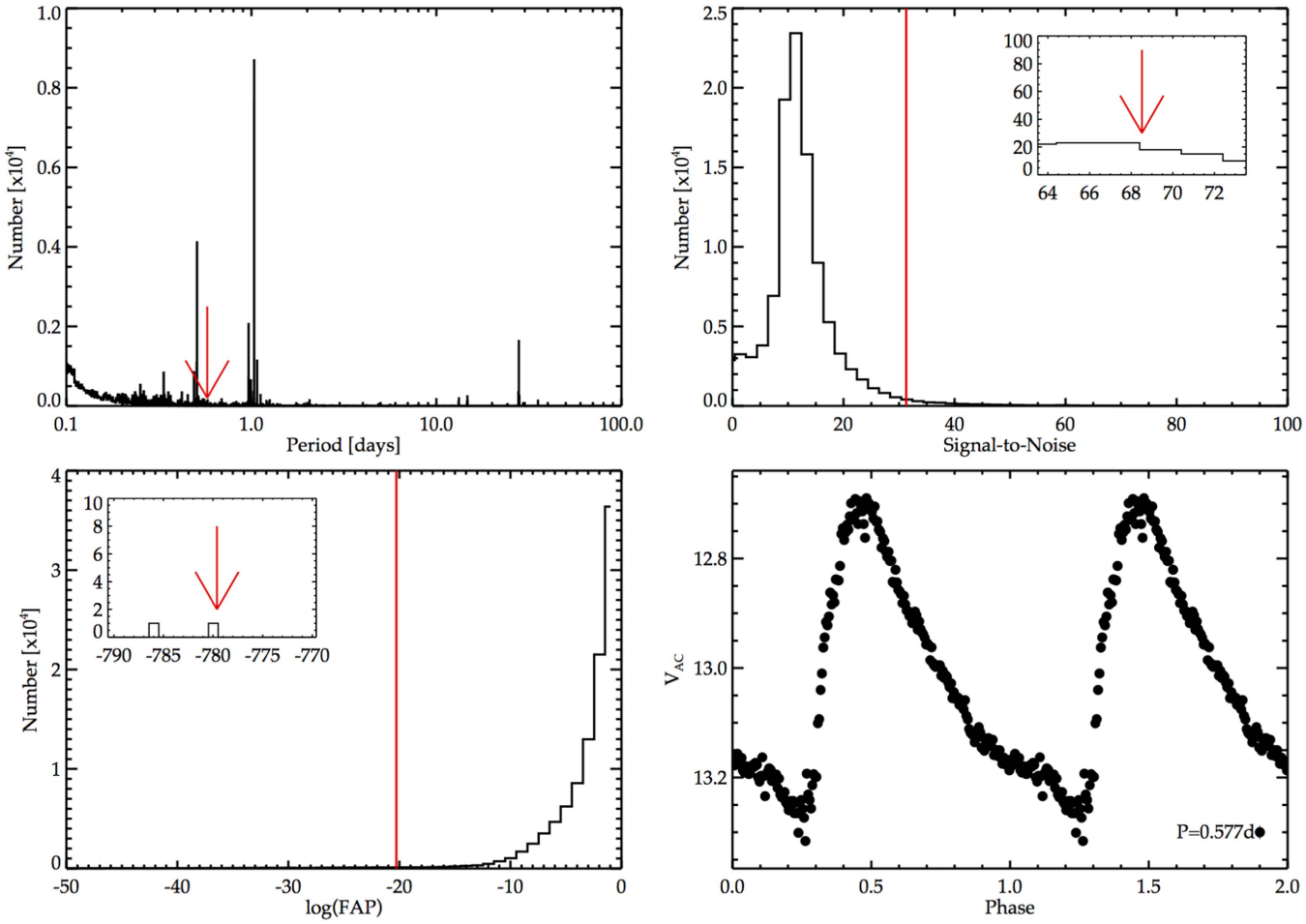

Figure 4. Periodicity tests used to identify periodic candidates in each young stellar association. Top left: the number of "periodic" stars with similar periods, indicative of aliasing. The passing candidate is shown with a red arrow. Note that the period is not found on or near a large distribution of other periods. Top right: the $+3\sigma$ cut (red line) on the signal-to-noise ratio. The passing candidate is shown with an arrow in the window insert. Bottom left: the -3σ cut (red line) on the false alarm probability. The passing candidate's $\log_{10}$(FAP) is shown with an arrow in the window insert; Bottom right: the light curve of a periodic variable star candidate U071728 (also shown in Figure 3). The light curve has been phase folded on the recovered period of 0.577 days, binned into 200 data points, and plotted twice for clarity. The typical error is shown at the bottom right of the panel.

regime in which we searched for exoplanets, we investigated the signal-detection-efficiency statistic (hereafter SDE) described in Kovács et al. (2002) to determine the significance level of each transit. Any transit candidate with a SDE statistic greater than four was considered significant. True transits should only show the systematic dimming of each light curve and not a systematic brightening or anti-transit. Burke et al. (2006) suggests a transit to anti-transit statistic $\Delta\chi^2/\Delta\chi^2_-$, where both the transit and anti-transit χ^2 values are compared. Stars with the statistic $\geqslant$1.0 were considered candidates. Finally, all candidates passing these statistics were visually inspected to confirm the eclipse-like variation. If the star was known to be PMS from a previous study (Rizzuto et al. 2015), then we allowed the star to fail one of the two statistics because its a priori membership made it a high-priority candidate. We refined each period by searching the first five harmonics of the BLS period in case the routine was triggering on the wrong frequency.

4.3. Higher Precision Photometric and Preliminary Spectroscopic Follow Up

Any transiting HJ or PMB candidate passing all of the significance tests described in Sections 4.1 and 4.2 was then subject to a series of follow up photometric observations. These observations are used to provide independent, higher precision transit and eclipse measurements. They also helped to confirm and refine the orbital period, depth, ephemeris, and duration for each eclipse. The time of secondary eclipse was probed to rule out large variations in flux, which would indicate a grazing EB or background blend. The higher angular resolution of the follow up telescopes also allowed us to determine any contamination from blending due to the coarser pixel scale ($6\farcs2\,\mathrm{pix}^{-1}$) of the *AggieCam*. These observations also provided color measurements which helped to identify spectral type, binary contamination in the HJ sample, and association membership.

The 1.54 m telescope at EABA provided 300+ hr of *BVRI* photometry to date, with further observations planned. The 0.8 m telescope at the McDonald Observatory provided 14 hr of BVRI photometry. The Las Cumbres Global Observatory Telescope Network (LCOGT) provided 30 hr of *gri* photometry from their 1 m facilities. The Texas A&M University campus observatory 0.5 m telescope provided 30 hr of *gri* photometry. Additionally, the 2.1 m telescope at the McDonald Observatory, coupled with the Sandiford Echelle Spectrograph (McCarthy et al. 1993; hereafter SES), provided 14 hr of initial spectroscopic follow up.

Table 3
Distribution of Significant Variable Periods

Timescale (days)	USco	η Cha	IC 2391
<1	851	95	1062
1–10	337	32	331
10–100	148	41	141
>100	112	16	18

5. RESULTS

5.1. Classical Variable and Periodic Stars

Employing the metrics described above, we identified over 1599 variable candidates across all 3 fields; 593 in USco, 689 in IC 2391 and 317 in η Cha. We determined a normalized variable star rate of $1.98 \pm 0.08 \times 10^{-4}$ ($1.38 \pm 0.07 \times 10^{-4}$, $2.22 \pm 0.08 \times 10^{-4}$) variable stars per sq. deg. in USco (η Cha, IC 2391). These rates are generally consistent with one another and with those of previous wide-field variable star searches (Wang et al. 2011, 2013; Oelkers et al. 2015, 2016).

Similarly, we found 3,184 stars showing significant periodicity using the cuts above. We found 240 (62; 127) stars with significant variability that also exhibited a periodic signal in USco (η Cha; IC 2391). Table 3 presents the number of stars in each field with periodic variations of different timescales. Figure 5 shows 15 candidate variable and periodic stars from all 3 fields.

5.1.1. Classification of Variable Stars

We classified each variable star with a general type using an IDL implementation of a k-means clustering algorithm, `CLUST_WTS` and `CLUSTER`. k-means clustering attempts to segregate features of each object into k-clusters to minimize the distance between each point in the cluster and the center of the cluster (MacQueen 1967). We selected six features of each variable star light curve to use in the clustering algorithm.

1. The magnitude difference between the mean magnitude of the first half of the light curve and the total mean magnitude.
2. The magnitude difference between the mean magnitude of the second half of the light curve and the total mean magnitude.
3. J, described in Section 4.1.
4. The skewness of the light curve.
5. The kurtosis of the light curve.
6. The LS period, if it was determined to be significant as described in Section 4.2.

Features 1 and 2 were selected to aid in identifying variable stars showing an overall increasing, decreasing or "constant" trend with time. Feature 3 was selected since its measure of variability is insensitive to light curve dispersion, as opposed to rms or Δ_{90}. Features 4 and 5 were selected to describe the uniformity of the change in magnitude around the mean magnitude (i.e., large constant oscillations or infrequent pulses). Finally, feature 6 was selected to aid in differentiating between long- or short-period variations.

The variable stars were clustered into one of five types using the features above. We found selecting more clusters made too many indistinguishable clusters and selecting fewer clusters grouped too many diverse objects.

1. Short-term, uniform periodic motion (i.e., RR Lyrae, contact, semi-detached, and short-period detached binaries, sinusoidal variables).
2. Infrequent variability (i.e., possible flares, long-period detached binaries, possible systematics).
3. Short-period, non-sinusoidal periodic variables.
4. Long-term, sinusoidal periodic variation.
5. Long-term, irregular variation.

Each variable star has been identified with its cluster membership in the final stellar library described in Table 2. We note that many stars in cluster 2 appear to show variation at identical times, likely due to systematics of the detector. We have elected to include them in our sample because they passed all of the variability cuts outlined in Section 4. We visually classified stars in clusters 1 and 2 to identify the eclipsing binary candidates described in Section 5.3.

5.2. Exoplanet Candidates and the Migration Timescale for Hot Jupiters

Previous observational studies of main-sequence stars have suggested the detection rate of a transiting HJ to be ~1 planet for every 5000 stars observed per month (Burke et al. 2006). Our survey was expected to extend far beyond the one-month time span required and we assumed we would detect multiple HJs. While each association does not contain the 5000 stars required to find one transiting HJ in one month's time, the planned survey duration of 3 years and knowledge of cluster members would allow selective targeting to determine the presence of young transiting HJs. It was also expected we would find transiting HJs around stars that have not yet been confirmed as cluster members due to the dearth of effective wide-field surveys of each association.

As a proof of concept, we injected transit signals for a variety of HJs with a range of periods ($0.5 < P < 10$ days) and radii ($0.8 < R_J < 2.0$) into simulated light curves with dispersions based on the typical rms limits of the detector and calculated the number of hours of observation required for a detection that passed the criteria outlined above. We used the published distance to each association and the 30 Myr isochrones from Pietrinferni et al. (2006) and calculated the stellar mass and radius for a range of apparent magnitudes. Figure 6 shows the results of this calculation for a 1.5 R_J with a period of 2.7 days. Taking into account long-term weather statistics for the site, we expected that after 18 months of observations we would be able to collect ~400 hr of data and achieve the required sensitivity over most of the target stellar types (F to early K). A further 18 months of observations would extend our sensitivity to the K/M boundary.

The combination of an unprecedented rainy season at EABA and equipment and server failures severely reduced our on-sky efficiency, and the survey was prematurely terminated after 15 months due to a lightning strike. Only ≈200 hr of observations were obtained. Our monthly efficiency rate is shown in Figure 6, along with the final survey numbers for each association (~100, 75, 40 hr for USco, η Cha, and IC 2391).

Even with our low number of observations, we identified seven possible planetary eclipse events as shown in Figure 7. We performed higher precision photometric follow up of each planetary candidate with LCOGT and EABA to confirm each eclipse and the expected ephemeris of mid-transit. We also used archive photometry from the *K2* Campaign 2 mission

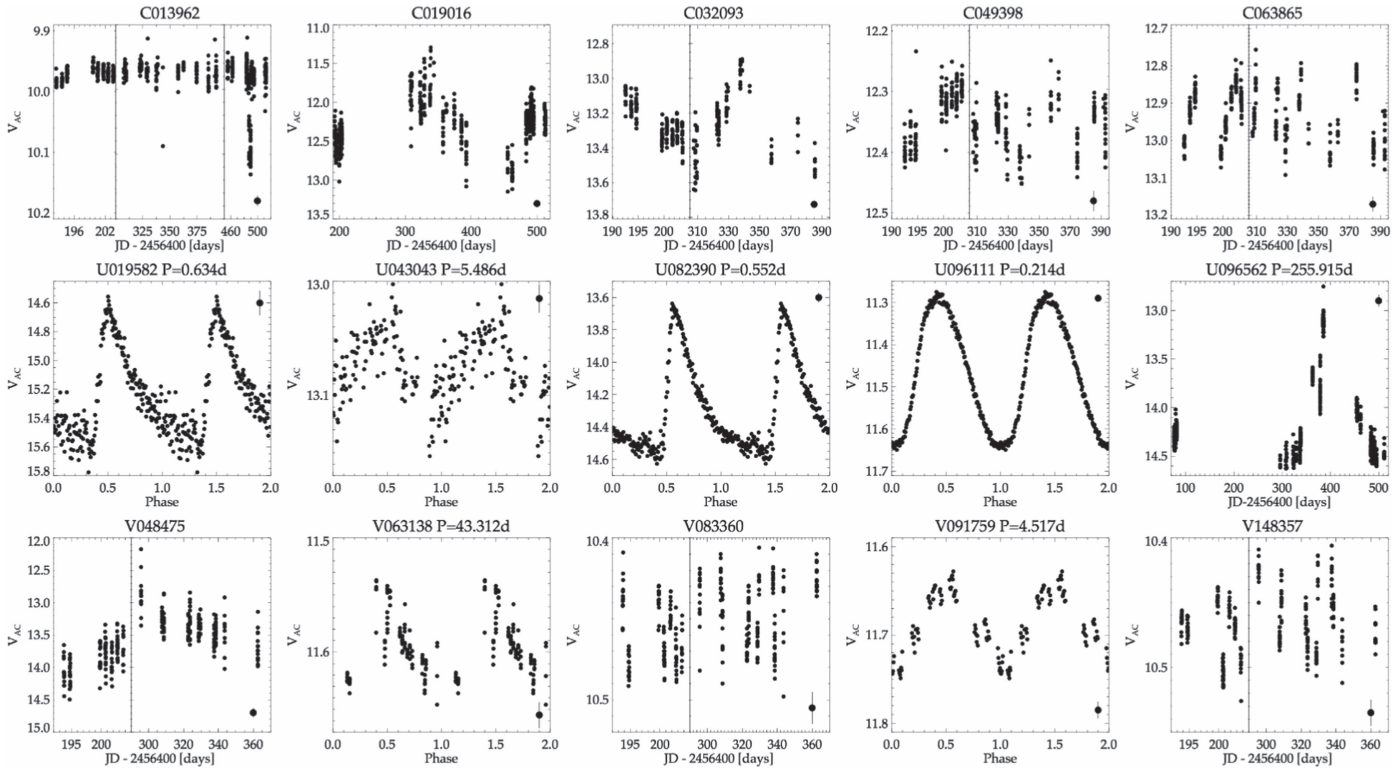

Figure 5. Fifteen variables found in each of the associations as part of our search. The period of the star is displayed in the title of the panel if it was identified as significant in our search. Panels in temporal space have been binned in 10 m intervals. Panels in phase space have been binned in 200 phase bins and plotted twice for clarity. Typical photometric error is plotted on the top or bottom right of each panel.

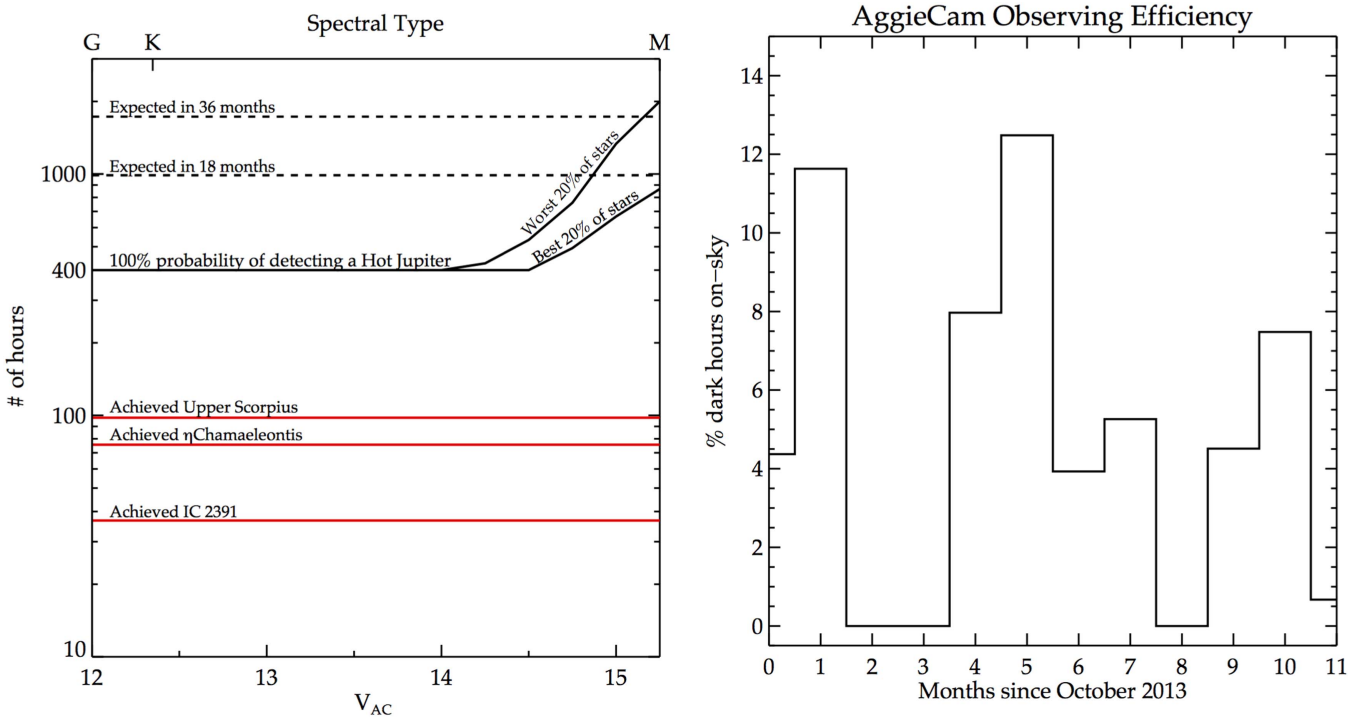

Figure 6. Left: the black line denotes the cumulative number of hours required to detect a transiting 1.5 R_J HJ with $P = 2.7$ days. The split in the black line marks the 20% of stars with the best and worst rms, respectively. The dotted lines mark our expected cumulative hours of observation prior to the survey. The red lines mark the achieved cumulative observed hours for each association. Right: percentage of dark hours that yielded useful data during each month of the *AggieCam* observing campaign since 2013 October. A combination of unprecedented weather conditions, coupled with technical failures, led to a low observing efficiency.

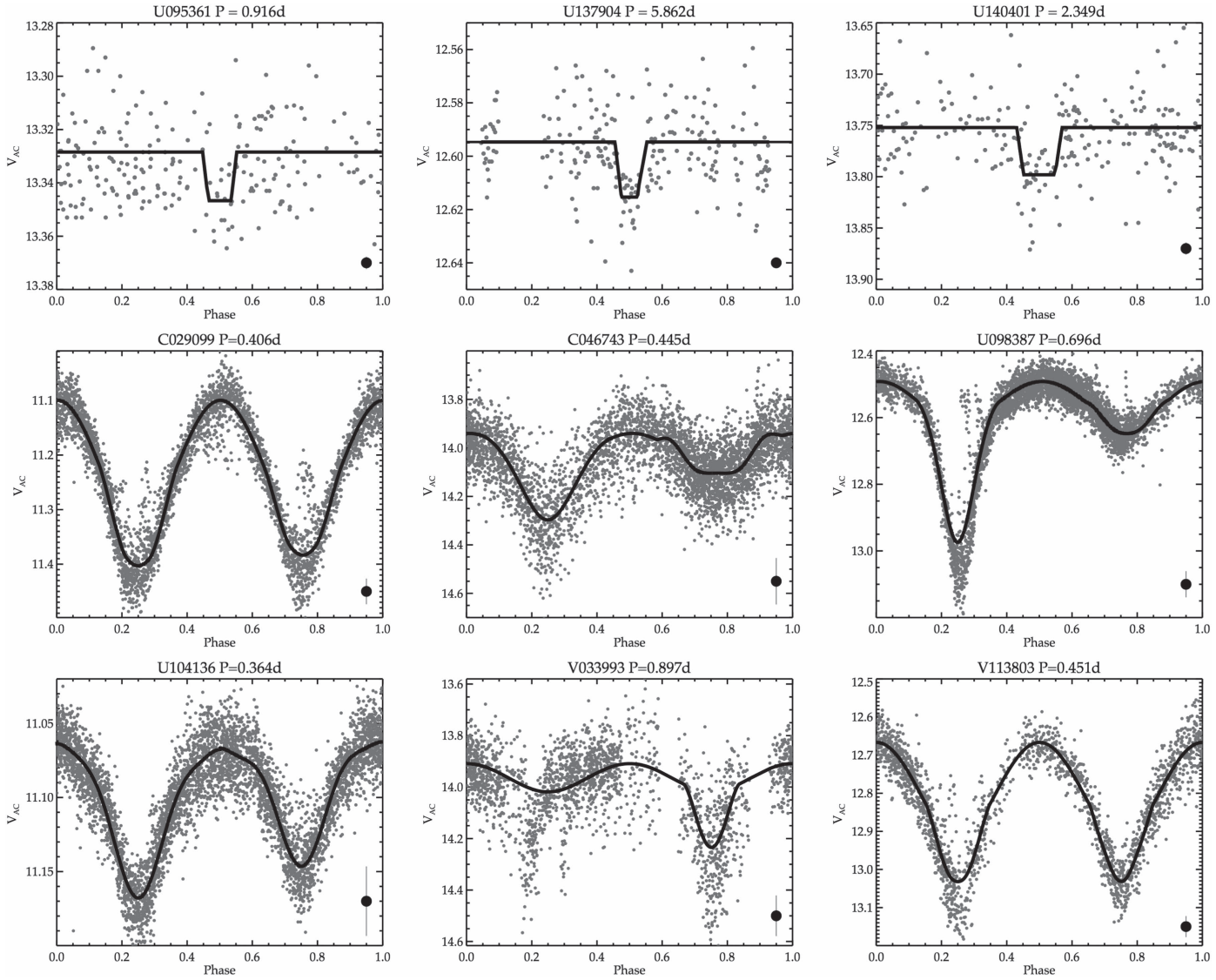

Figure 7. Top Row: three HJ candidates of various periods, detected at high significance as part of our search. The HJ candidate light curves have been binned into 30 m bins and phase folded. The black line denotes the best-fit BLS model of the transit (Bakos et al. 2002). Middle and bottom rows: six PMB candidates from each association. The black lines denote the best-fit JKTEBOP model (Southworth et al. 2013). Errors are shown in the bottom right of each figure.

Table 4
Hot Jupiter Candidates

Star ID	Coordinates		BLS Period	BLS Ephemeris	Mag.	Depth	Follow up
	R.A. (hr)	Decl. (deg)	(days)	JD-24546400	V_{AC}	(mmag)	Observatory
U022979	16:15:39.5	−24:55:41	0.818758	76.631834	13.407	27	Bosque Alegre
U064813	16:08:35.9	−23:55:39	0.706294	77.273527	12.737	28	LCOGT
U095361	16:04:06.7	−26:37:07	0.915534	77.040402	13.331	16	LCOGT
U120649	16:00:07.3	−26:16:46	1.493101	76.612173	14.197	28	Bosque Alegre
U137904	15:57:16.7	−25:29:19	5.861766	80.164762	12.597	17	*K2*
U140401	15:56:55.5	−22:58:40	2.349168	77.197127	13.754	42	Bosque Alegre
C067591	07:50:41.6	−78:43:34	0.251447	192.535710	13.463	29	Bosque Alegre

(Howell et al. 2014). Unfortunately, we were unable to recover the eclipse events at the expected ephemeris times. We have included a list of each of the candidates and their determined orbital information for completeness in Table 4.

We need to properly assess our ability to detect these objects and identify any potential biases before we can speculate on the scientific implications of our null result. We will make this interpretation for USco *only*, because of the significantly larger number of candidates recovered (6) and the larger number of observed hours compared to η Cha and IC 2391. We will do this by answering two questions to determine the confidence on our null result: (1) How many

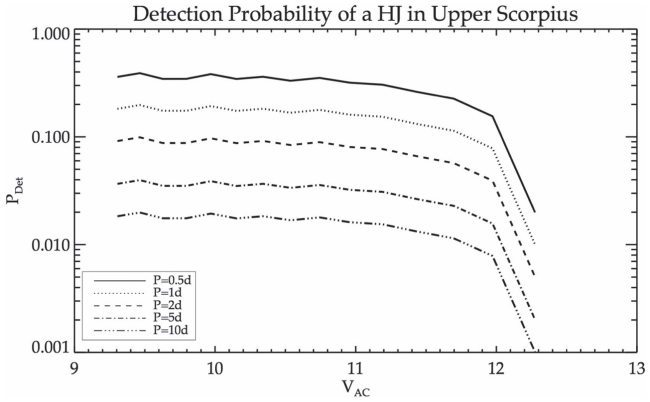

Figure 8. Probability of detecting a HJ in our sample as a function of magnitude for stars in USco. The probability of detecting a HJ with $P < 0.5$ days is ∼34% for $V_{AC} < 12$ and quickly declines for longer periods and fainter magnitudes.

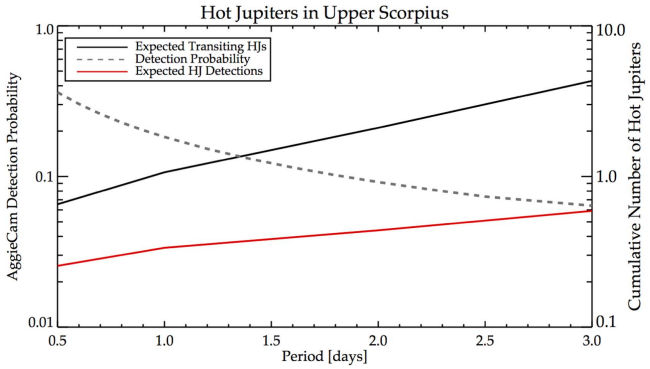

Figure 9. Cumulative number of expected HJs in the USco association as a function of period. The black line denotes the number of HJs detected with 100% efficiency while the red line denotes our expected detection rate. The gray dashed line is our detection efficiency as a function of orbital period. At $P = 0.5$ days where, we are most likely to detect planets, we find our null result is consistent with expectation that <1 HJ would exist with such a period.

HJs should exist in this associations? (2) If a HJ exists, would we have detected it?

5.2.1. How Many Hot Jupiters Should Exist in this Association?

Previous studies of main-sequence stars have determined the planet fraction of HJs is $P_{\rm frac} \approx 1\%$. However, the expectations for Very Hot Jupiters ($P < 3$ days) are $P_{\rm frac} \approx 0.1\%$ (Hartman et al. 2008; Bayliss & Sackett 2011; Fressin et al. 2013). Given the target associations have 100–1000 confirmed members, extra care needs to be given to interpreting our null result. By combining these planet fractions with the detection probabilities below, we can determine if our null result is consistent with the expectation of HJ migration due to disk interactions.

5.2.2. If a Hot Jupiter Exists, Would We Have Detected it?

We determine our detection probability following the same logic as Burke et al. (2006), with the full detection probability being defined as

$$P_{\rm det,i} = \int\int \frac{d^2p}{dR_p da} P_{\epsilon,i}(a, R_p) P_{T,i}(a, R_p) P_{\rm mem,i} dR_p da, \quad (3)$$

where R_p is defined as the planet radius; a is the semimajor axis; $P_{\epsilon,i}(a, R_p)$ is the probability of detecting a transit around the ith star in the survey averaged over orbital phase and inclination; $P_{T,i}(a, R_p)$ is the probability a planet of R_p and a would transit its host star; $P_{\rm mem,i}$ is the probability the ith star is a member of the association.

We calculate $P_{\epsilon,i}$ following the logic of Gaudi (2000) and integrate over the survey's achieved photometric precision, achieved observing cadence and the minimum threshold to detect HJs of various periods ($0.5 < P < 10$ days) and radii ($0.8 < R_J < 2$). The calculation of $P_{T,i}$ is independent of our survey data. If we assume a random inclination orientation of a star with respect to the observer, then $P_{T,i} = \frac{R_* + R_p}{a}$, where R_* is the radius of the star. We assumed a uniform distribution of inclination angles for our calculation. We integrated these detection limits over all stars in our FOV because we were also interested in detecting planets around non-association members, if they existed.

5.2.3. Implications of the Null Result

If we have not detected any HJs because they have not yet migrated, and its not simply an artifact of the low number of observations, we can attempt to understand the implications for the migration timescale. Because disk formation, accretion and dissipation is expected to be finished by 10 Myr, it is surprising the planets have not yet migrated to their "Hot" positions. Both Type I and II migration require an actively accreting disk to move the planet inwards toward its host star (Ida & Lin 2008). Similarly, recent studies have also suggested in situ HJ formation and that the snow line may not be a requirement for primary atmosphere retention (Batygin et al. 2015).

Recent work by Mann et al. (2016) has shown the detection of a ∼5 $R_\oplus$ "Hot Neptune" with an orbital period of ∼5.4 days orbiting an 11 Myr, M3 star in USco. While the star is not in our FOV, it is unlikely we would have detected the eclipse given the parameters of the system. The star's apparent magnitude is 15.5 in V and the planet transits with a ∼0.003 mag eclipse depth (we transformed APASS g&r to V using the relations from Lupton et al. 2005; APASS V for this star was determined to be unreliable; Henden et al. 2012). The AggieCam's precision at this magnitude is >0.1 mag (see Figure 2). We also have a very low recovery rate for periods greater than 1.0 days (see Figure 8) and our null detection at these periods matches the expectation for these objects in this field (see Figure 9). Similarly, Johns-Krull et al. (2016) have identified a HJ candidate ($P \sim 9$ days) through optical and infrared radial velocity measurements of the PMS star CI Tau (2 Myr). These detections provide evidence that disk migration is the driving force for gas-giant migration at early times (<11 Myr) and helps to confirm the observations of previously discovered young, transiting, "hot" gas-giants (van Eyken et al. 2012). These detection also imply we did not detect a HJ only because we failed to reach our desired temporal coverage of the field and not because these objects have failed to migrate before 11 Myr.

5.3. Binary Candidates and Membership Confidence Testing

Our survey yielded 346 PMB candidates; 151 in USco, 138 in IC 2391, and 57 in η Cha. All of these objects require higher precision photometric and spectroscopic follow up

Table 5
Binary Candidate Testing

Young Stellar Association	Effective Temperatures & Separations	Proper Motions [UCAC4]	Infrared Excess [2MASS and *WISE*]	Total Number of Candidates
USco	134	45	11	151
IC 2391	131	55	21	138
η Cha	47	10	9	57

Table 6
Pre-main-sequence Eclipsing Binary Candidates

AggieCam ID	Coordinates		Magnitude	Period	Metrics		
	R.A. (hr)	Decl. (deg)	V_{AC}	(days)	ET	IR	PM
V089825	08:39:01.00	−53:50:25	13.442	2.025352	1	3	3
V130033	08:41:57.79	−52:31:33	12.108	0.808794	1	1	3
V065240	08:48:14.21	−54:30:25	15.076	0.961662	1	1	3
U077182	16:06:53.44	−26:49:19	15.019	0.535817	1	2	2
V033325	08:38:49.10	−55:36:27	13.121	0.225700	1	2	2
V096596	08:28:07.54	−53:40:02	12.045	2.271902	1	1	3
V105161	08:54:43.25	−53:15:18	14.289	0.821764	1	2	2
V152845	08:33:58.26	−51:32:17	11.418	5.413995	1	3	0
V167741	08:24:08.44	−50:55:27	12.747	10.897848	1	0	3
V106482	08:23:40.70	−53:20:25	11.745	1.804665	1	3	0
V077746	08:53:21.85	−54:03:24	13.848	1.250303	1	0	3
U104136	16:02:38.25	−24:01:52	11.100	0.364308	1	0	3
C105839	08:02:16.16	−77:00:14	13.275	0.881469	1	3	0
U098597	16:03:30.09	−24:31:47	11.043	5.061739	1	0	3
V105749	08:33:29.74	−53:21:17	14.790	1.693400	1	0	3
V152442	08:26:58.84	−51:33:55	14.116	0.211067	1	3	0
V087571	08:37:16.21	−53:53:02	13.046	1.961866	1	0	3
V142813	08:46:07.25	−51:52:21	14.176	1.257733	1	3	0
V095317	08:27:57.28	−53:40:32	12.327	0.437948	1	3	0
U098050	16:03:36.56	−25:09:13	12.276	1.034986	1	0	3
U056279	16:10:04.17	−26:25:49	12.443	6.114638	1	0	3

Note. ET metric denotes stars with effective temperature and separations plausible at the distance of the cluster. The IR flag denotes how many IR excesses were identified in the 2MASS and *WISE* photometry. PM denotes stars with proper motions consistent with the moving group to 1–3σ.

(This table is available in its entirety in machine-readable form.)

for firm classification and accurate determination of stellar parameters. Since the spectroscopic follow up of more than 300 objects is not a trivial task, we ranked the candidates by priority on a scale of 0 (low) to 7 (high). We calculated the ranking using archival 2MASS and *WISE* colors to determine infrared excesses (Skrutskie et al. 2006; Wright et al. 2010), using the UCAC4 proper motion catalog to compare the motion of a given candidate with the mean of its putative association (Zacharias et al. 2013), inferring possible component masses based on eclipse depth and apparent magnitude and high-resolution spectroscopy to search for the Li I line at 6708 Å for seven initial test binaries. The final results of these tests are shown in Table 5 and the complete list of pre-main-sequence eclipsing binary candidates can be found in Table 6.

5.3.1. Color Selections

An infrared excess is used to describe an object which appears to have a normal spectral energy distribution in the ultraviolet and visible wavelengths but shows a large excess of flux at infrared wavelengths. These excesses manifest themselves in young stellar objects because these stars are typically enshrouded in a dusty proto-stellar disk which absorbs ultraviolet light and re-emits it in the infrared.

To determine which stars may show these infrared excess, we investigate the 2MASS and *WISE* archival photometry (Skrutskie et al. 2006; Wright et al. 2010). We combined the $J-H$ versus $H-K$ color–color diagram with the stellar locus provided by Pecaut & Mamajek (2013) to estimate the spectral type of each binary. If the star was within 2σ of a particular point in the locus we deemed the photometry to be accurate enough to estimate the spectral type.

Following the methodology of Luhman & Mamajek (2012) and Rizzuto et al. (2015), we made color cuts using photometry in the 2MASS K_s and the *WISE* W2, W3, and W4 bands. Stars lying above the lines denoted in Figure 10 are flagged as showing infrared excesses indicative of a younger stellar population. These boundaries are calculated based on the expected photospheric flux observable *after* dissipation of the proto-planetary disk. Binaries showing these excesses were flagged as high-priority candidates, with each excess adding an additional point to the total priority score. We found 11 (10, 21)

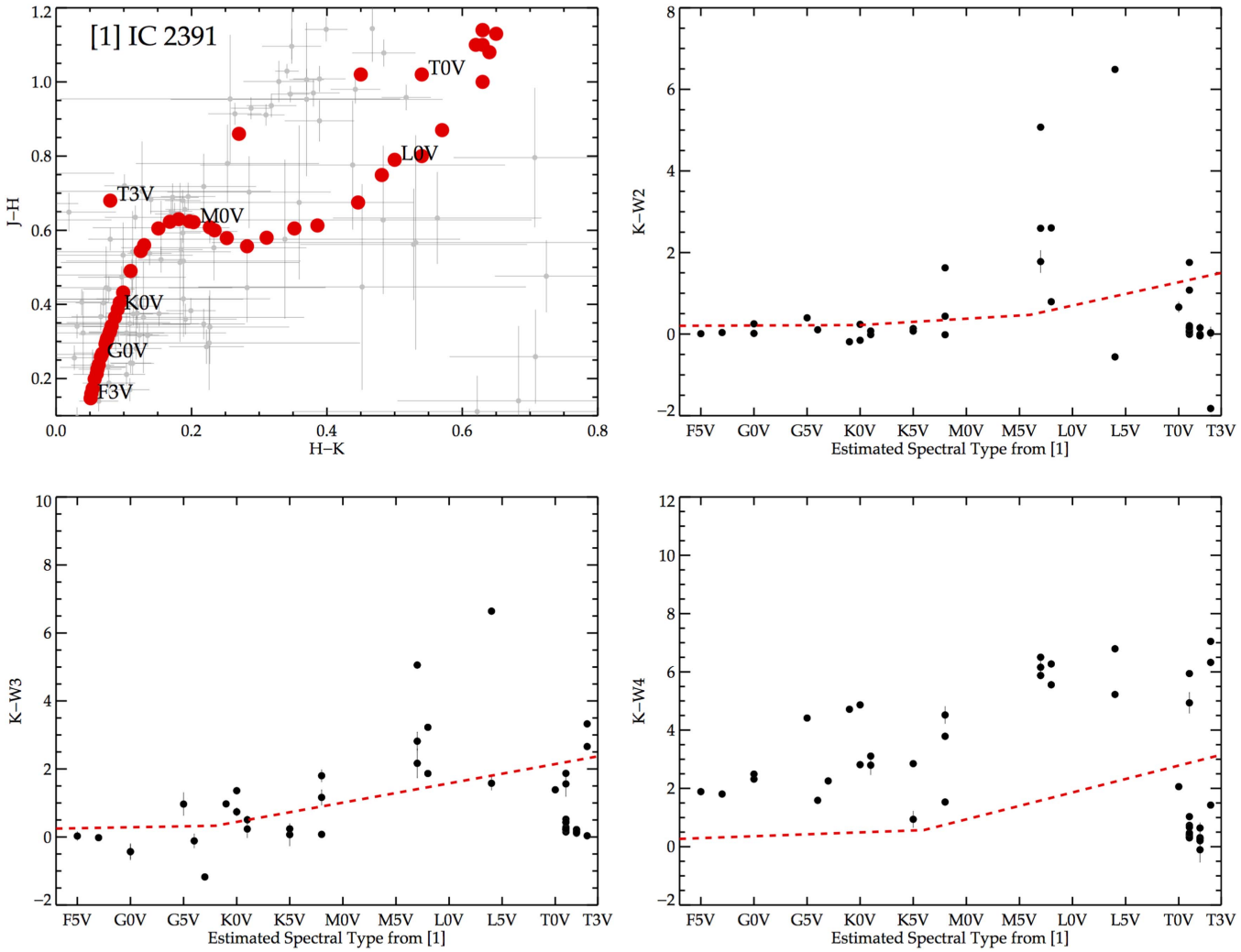

Figure 10. Infrared excesses of IC 2391. Top left: 2MASS color–color diagram and stellar locus from Pecaut & Mamajek (2013). Stars were assigned with a specific spectral type if they were located within 2σ of a particular data point in the locus. Top right, bottom left, and bottom right: (K-W2 (W3, W4)) vs. estimated spectral type diagram. Stars lying above the red lines are considered to have an excess amount of flux in the infrared, indicative of an accretion disk. The red dotted line marks where the expected photospheric excess ends for main-sequence objects (Luhman & Mamajek 2012; Rizzuto et al. 2015).

stars in USco (η Cha, IC 2391) to have at least 1 infrared excess.

5.3.2. Proper Motions

We used the proper motions from the UCAC4 catalog (Zacharias et al. 2013) to identify objects which show similar motions to the well studied O/B/A/F stars in each association. Using the measured mean proper motions of each association from previous studies (Dodd 2004; Luhman & Mamajek 2012; Lopez Martí et al. 2013) and the expected 15–20 mas error of the UCAC4 catalog, we identified all candidate binaries which were within 3σ of the mean proper motion. Only stars with measured proper motions were included in our significance testing. We increased the priority score for each candidate based on the difference, in σ, between the star's proper motion and the mean of the association as follows: $\Delta\mu < 1\sigma = +3$; $1\sigma < \Delta\mu < 2\sigma = +2$; $2\sigma < \Delta\mu < 3\sigma = +1$; $\Delta\mu > 3\sigma = 0$. If the candidate had no measured proper motion, it was given no points. We found 45 (10, 55) stars in USco (η Cha, IC 2391) to have a proper motion within 3σ of the proper motion of the cluster. Figure 11 shows measured proper motions for the binary candidates in η Cha and their positions in the *AggieCam* FOV.

5.3.3. Testing Viable Binary Components

The component masses of the system can still be estimated even without proper spectroscopic observations. The ratio of the eclipse depths is proportional to the fourth-root of the ratio of the temperatures of the photospheres of the stars. This ratio can then be used in conjunction with the apparent magnitude and the distance to the association to place limits on the masses of the components, under the assumption that the object is a *bona-fide* member.

We fit a parabola to both the primary and secondary eclipses using the IDL routine `POLY_FIT` to determine the minimum flux value. We then calculated the ratio of the effective temperatures as follows:

$$\left(\frac{T_S}{T_P}\right)^4 = \frac{F_0 - F_P}{F_0 - F_S}, \quad (4)$$

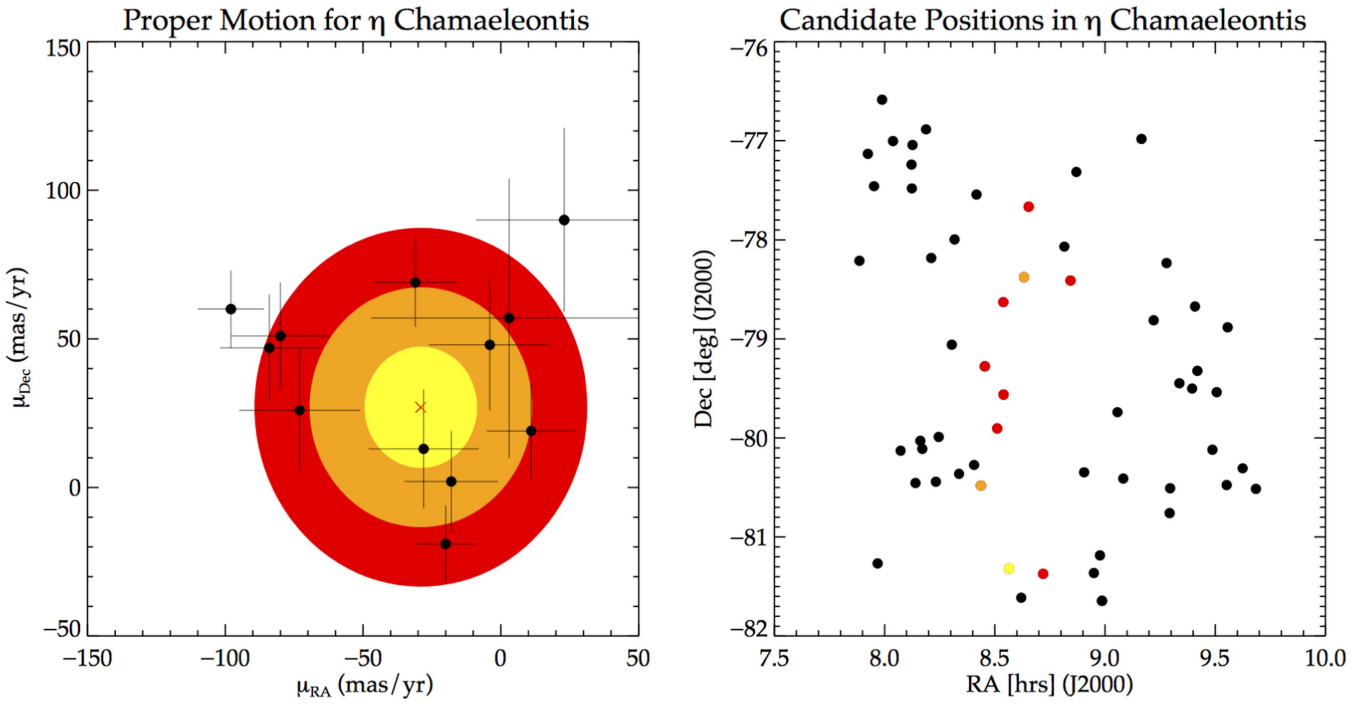

Figure 11. Left: the measured proper motions of stars in the η Cha field with measured proper motions from the UCAC4 catalog plotted with their 1σ error bars. Objects were selected as likely candidates based on their position relative to the mean proper motion of the moving group. The colored regions denote 1, 2, and 3σ errors of the UCAC4 catalog (yellow, orange, and red, respectively). Right: the position of each PMB candidate in the FOV of the *AggieCam*. The coloring of the points relates to the proximity of the proper motion of a given star to the mean of the association. A black dot means the star either was too far from the mean motion or did not have a proper motion in UCAC4.

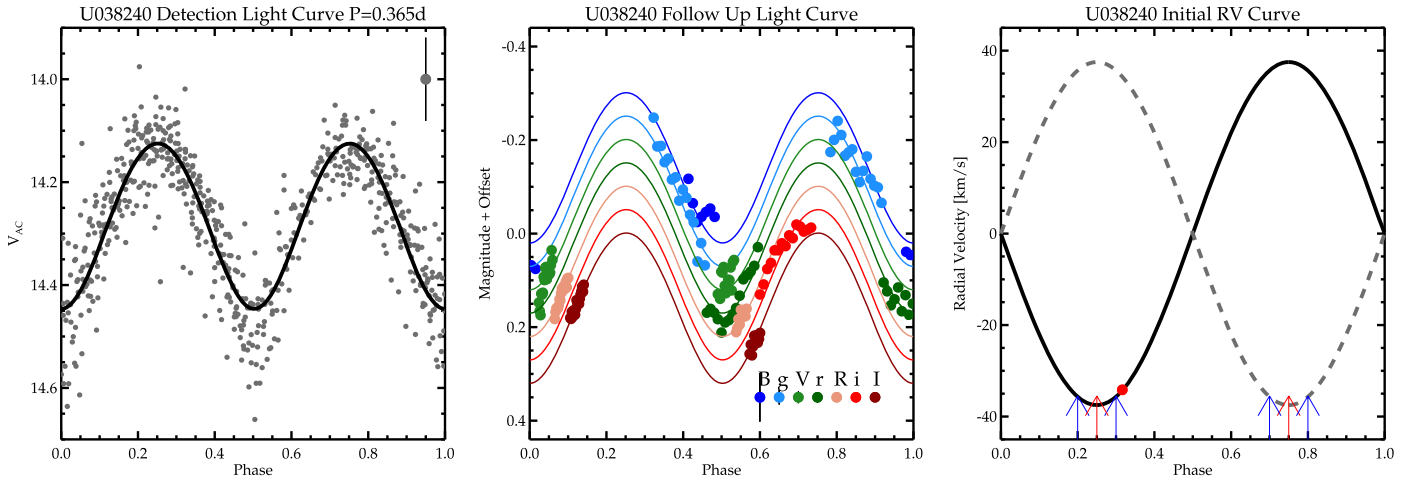

Figure 12. PMB candidate U038240 discovered in USco at each stage of the classification process: detection (top); multi-color follow up (middle); initial RV measurements (bottom). The solid lines denotes the best-fit JKTEBOP models (Southworth et al. 2013). The expected RV variation is extrapolated from the eccentricity of the system and the best-fit orbital parameters of JKTEBOP. The blue arrows denote the acceptable range of observation in phase and the red arrows denote exact quadrature.

where F_0 is the flux at quadrature and F_P and T_P are the flux during the primary eclipse and effective temperature of the primary star respectively (an S denotes the secondary).

The distance modulus to each association was subtracted from the apparent magnitudes to determine the expected absolute magnitude of each candidate. The Spada et al. (2013) zero-age-main-sequence isochrones were employed to calculate the magnitudes of the components that could be combined to generate this magnitude based on the temperature ratio. *Kepler*'s Third Law was used to calculate the separation of the system using the known period. We determined the viability of each binary based on the orbital separation and the shape of the light curve. For example, a binary composed of two K-dwarfs with a separation of 1 solar radius should be in a nearly contact system and *not* a detached system. If the system was deemed viable it was given one point toward its priority score. We found 134 (47, 131) stars in USco (η Cha, IC 2391) to have viable binary components for their expected distance.

5.3.4. Spectroscopy

Preliminary spectroscopy was obtained for seven PMB candidates at the McDonald Observatory during the Spring of 2015. The combination of spread in ephemeris timing and poor observing conditions only allowed each PMB to be observed once, close to quadrature. Nevertheless, these measurements provide valuable information about the radial velocity and spectral types for each system. We obtained the spectra using the SES on the 2.1 m at the McDonald Observatory. Th-Ar exposures bracketed the science observations and were used to wavelength-calibrate the data using the IRAF routine `REFSPEC`. The radial velocities were calculated using a cross-correlation with reference spectra taken on the same night and spectral templates from SDSS DR5 (Adelman-McCarthy et al. 2007). While the SNR of our spectra were not very high (<10), we nevertheless achieved 1–5 km s^{-1} precision on the radial velocity measurements. The low SNR prevented any detection of Li 6708 Å.

We then subjected the detection light curve, follow up multi-color photometry, and initial estimates of the radial velocity to the JKTEBOP binary-fitting program (Southworth et al. 2013). JKTEBOP models each component of a binary as a sphere for calculating the eclipse shapes and a biaxial ellipsoid for calculating proximity effects. The program uses Levenberg-Marquardt optimization to find the best-fit model. An example of a binary being subjected to this fitting process is shown in Figure 12.

6. CONCLUSIONS

Although our observations were plagued by bad weather, technical setbacks, and a lightning strike, we were able to reach the necessary precision for an exoplanet and eclipsing binary survey. We detected 346 eclipsing pre-main-sequence binary candidates and identified 7 candidate transiting Hot Jupiters; the latter were ruled out with higher precision follow up observations. Additionally, we identified and categorized 4354 variable and periodic stars across the 3 target associations.

In order to properly interpret our null result, we determined our detection probability to be 34% for HJs with $P < 0.5$ days. Recent work by Mann et al. (2016) has identified a "Hot Neptune" transiting a PMS star in USco, thereby providing evidence for disk migration and suggesting we could have detected transiting planets if we had obtained sufficient temporal coverage of each field.

Finally, we identified 346 candidate pre-main-sequence binaries. 12% of these stars show an infrared excess, 32% of these stars have proper motions consistent with their putative association and 90% have temperature ratios which are consistent with two zero-age-main-sequence stars at the distance of the respective association. We found 74 PMB candidates to have a priority score of 3 or more, denoting a high-likelihood of being pre-main-sequence binaries and have prioritized them for follow up observations.

R.J.O. and L.M.M. acknowledge financial support from the George P. and Cynthia Woods Mitchell Institute for Fundamental Physics and Astronomy and the Mitchell-Heep-Munnerlyn Endowed Career Enhancement Professorship in Physics or Astronomy. They also thank the observing staff at the Estación Astrofisíca de Bosque Alegre and the Observatorio Astronomica de Córdoba; specifically Pablo Guzzo, Cecilia Quiñones and Luis Tapia. R.J.O. thanks Daniel Nagasawa and Lucas Turner for their support during the McDonald observing runs, Dr. James Long for the useful discussion on the proper interpretation of a null hypothesis, and Don Carona for his help at the Texas A&M Campus Observatory. K.M.S. was supported by NSF grant AST-1263034, "REU Site: Astronomical Research and Instrumentation at Texas A&M University." This work makes use of observations from the LCOGT network. Finally, the authors would like to acknowledge the LCOGT TAC for the generous amount of telescope time provided.

REFERENCES

Adelman-McCarthy, J. K., Agüeros, M. A., Allam, S. S., et al. 2007, ApJS, 172, 634
Alard, C. 2000, A&AS, 144, 363
Alard, C., & Lupton, R. H. 1998, ApJ, 503, 325
Anderson, K. R., Storch, N. I., & Lai, D. 2016, MNRAS, 456, 3671
Baglin, A., Michel, E., Auvergne, M. & COROT Team 2006, in ESA Special Publication, Vol. 624, Proc. SOHO 18/GONG 2006/HELAS I, Beyond the Spherical Sun, ed. K. Fletcher, 34.1
Bakos, G. Á, Lázár, J., Papp, I., Sári, P., & Green, E. M. 2002, PASP, 114, 974
Baraffe, I., Homeier, D., Allard, F., & Chabrier, G. 2015, A&A, 577, A42
Batygin, K., Bodenheimer, P. H., & Laughlin, G. P. 2015, arXiv:1511.09157
Bayliss, D. D. R., & Sackett, P. D. 2011, ApJ, 743, 103
Bessell, M. S. 1990, PASP, 102, 1181
Borucki, W. J., Koch, D., Basri, G., et al. 2010, Sci, 327, 977
Burke, C. J., Gaudi, B. S., DePoy, D. L., & Pogge, R. W. 2006, AJ, 132, 210
Charbonneau, D., Brown, T. M., Latham, D. W., & Mayor, M. 2000, ApJL, 529, L45
Ciardi, D. R., van Eyken, J. C., Barnes, J. W., et al. 2015, ApJ, 809, 42
Dodd, R. J. 2004, MNRAS, 355, 959
Duchon, J. 1976, ESAIM: Mathematical Modelling and Numerical Analysis—Modélisation Mathématique et Analyse Numérique, 10, 5
Fressin, F., Torres, G., Charbonneau, D., et al. 2013, ApJ, 766, 81
Gaudi, B. S. 2000, ApJL, 539, L59
Hartman, J. D., Gaudi, B. S., Holman, M. J., et al. 2008, ApJ, 675, 1254
Hartman, J. D., Stanek, K. Z., Gaudi, B. S., Holman, M. J., & McLeod, B. A. 2005, AJ, 130, 2241
Henden, A. A., Levine, S. E., Terrell, D., Smith, T. C., & Welch, D. 2012, JAVSO, 40, 430
Henry, G. W., Marcy, G. W., Butler, R. P., & Vogt, S. S. 2000, ApJL, 529, L41
Howell, S. B., Sobeck, C., Haas, M., et al. 2014, PASP, 126, 398
Ida, S., & Lin, D. N. C. 2008, ApJ, 673, 487
Johns-Krull, C. M., McLane, J. N., Prato, L., et al. 2016, arXiv:1605.07917
Johnson, H. L., & Morgan, W. W. 1953, ApJ, 117, 313
Kaluzny, J., Stanek, K. Z., Krockenberger, M., et al. 1998, AJ, 115, 1016
Kamiaka, S., Masuda, K., Xue, Y., et al. 2015, PASJ, 67, 94
Kennicutt, R. C., & Evans, N. J. 2012, ARA&A, 50, 531
Kovács, G., Bakos, G., & Noyes, R. W. 2005, MNRAS, 356, 557
Kovács, G., Zucker, S., & Mazeh, T. 2002, A&A, 391, 369
Kraus, A. L., Cody, A. M., Covey, K. R., et al. 2015, ApJ, 807, 3
Landolt, A. U. 1992, AJ, 104, 340
Lomb, N. R. 1976, Ap&SS, 39, 447
Lopez Martí, B., Jimenez Esteban, F., Bayo, A., et al. 2013, A&A, 551, A46
Luhman, K. L., & Mamajek, E. E. 2012, ApJ, 758, 31
Lupton, R. H., Jurić, M., Ivezić, Z., et al. 2005, BAAS, 37, 1384
MacQueen, J. 1967, in Proc. Fifth Berkeley Symposium on Mathematical Statistics and Probability, Vol. 1: Statistics (Berkeley, CA: Univ. California Press), 281
Mamajek, E. E. 2009, in AIP Conf. Ser. 1158, ed. T. Usuda, M. Tamura, & M. Ishii (Melville, NY: AIP), 3
Mamajek, E. E., Lawson, W. A., & Feigelson, E. D. 1999, ApJL, 516, L77
Mann, A. W., Newton, E. R., Rizzuto, A. C., et al. 2016, arXiv:1604.06165
Mayor, M., & Queloz, D. 1995, Natur, 378, 355
McCarthy, J. K., Sandiford, B. A., Boyd, D., & Booth, J. 1993, PASP, 105, 881
Miller, J. P., Pennypacker, C. R., & White, G. L. 2008, PASP, 120, 449
Morales-Calderón, M., Stauffer, J. R., Stassun, K. G., et al. 2012, ApJ, 753, 149
Oelkers, R. J., Macri, L. M., Wang, L., et al. 2015, AJ, 149, 50
Oelkers, R. J., Macri, L. M., Wang, L., et al. 2016, AJ, 151, 166
Pecaut, M. J., & Mamajek, E. E. 2013, ApJS, 208, 9
Pecaut, M. J., Mamajek, E. E., & Bubar, E. J. 2012, ApJ, 746, 154

Pepper, J., Pogge, R. W., DePoy, D. L., et al. 2007, PASP, 119, 923
Pietrinferni, A., Cassisi, S., Salaris, M., & Castelli, F. 2006, ApJ, 642, 797
Pollacco, D. L., Skillen, I., Collier Cameron, A., et al. 2006, PASP, 118, 1407
Preibisch, T., Brown, A. G. A., Bridges, T., Guenther, E., & Zinnecker, H. 2002, AJ, 124, 404
Press, W. H., Teukolsky, S. A., Vetterling, W. T., & Flannery, B. P. 1992, Numerical Recipes in C. The Art of Scientific Computing (Cambridge: Cambridge Univ. Press)
Reipurth, B. 2008, Handbook of Star Forming Regions, Vol. II: The Southern Sky (San Francisco, CA: ASP)
Rizzuto, A. C., Ireland, M. J., & Kraus, A. L. 2015, MNRAS, 448, 2737
Scargle, J. D. 1982, ApJ, 263, 835
Skrutskie, M. F., Cutri, R. M., Stiening, R., et al. 2006, AJ, 131, 1163
Southworth, J., Mancini, L., Browne, P., et al. 2013, MNRAS, 434, 1300
Spada, F., Demarque, P., Kim, Y.-C., & Sills, A. 2013, ApJ, 776, 87
Stassun, K. G., Feiden, G. A., & Torres, G. 2014, NewAR, 60, 1
Stetson, P. B. 1987, PASP, 99, 191
Stetson, P. B. 1996, PASP, 108, 851
Torres, G., Andersen, J., & Giménez, A. 2010, A&ARv, 18, 67
van Eyken, J. C., Ciardi, D. R., von Braun, K., et al. 2012, ApJ, 755, 42
Wang, D., Foreman-Mackey, D., Hogg, D. W., & Schölkopf, B. 2015, arXiv:1508.01853
Wang, L., Macri, L. M., Krisciunas, K., et al. 2011, AJ, 142, 155
Wang, L., Macri, L. M., Wang, L., et al. 2013, AJ, 146, 139
Wright, E. L., Eisenhardt, P. R. M., Mainzer, A. K., et al. 2010, AJ, 140, 1868
Young, A. T. 1967, AJ, 72, 747
Yu, L., Winn, J. N., Gillon, M., et al. 2015, ApJ, 812, 48
Zacharias, N., Finch, C. T., Girard, T. M., et al. 2013, AJ, 145, 44
Zechmeister, M., & Kürster, M. 2009, A&A, 496, 577